An analytical model for top-hat long transient mode-mismatched thermal lens spectroscopy

M. Sabaeian
sabaeian@scu.ac.ir
Physics Department, Faculty of Science, Shahid Chamran University of Ahvaz, Ahvaz, 61357-43135, Iran

H. Rezaei
Physics Department, Faculty of Science, Shahid Chamran University of Ahvaz, Ahvaz, 61357-43135, Iran

It has been shown that a top-hat excitation beam gives rise to a more sensitive signal for the thermal lens spectroscopy (TLS). Recently, a numerical model has been presented for a top- hat excitation beam in a dual-beam mod-mismatched TLS [Opt. Lett. 33(13), 1464-1466 (2008)]. In this work, we present a full analytical version of this model. Our model was based on a new solution of time-dependent heat equation for a finite radius cylindrical sample exposed to a top-hat excitation laser beam. The Fresnel diffraction integration method was then used to calculate on-axis probe-beam intensity variations due to thermal lensing by taking the aberrant nature of the thermal lens into account. The model was confirmed with experimental data of LSCAS-2 with an excellent agreement.
[DOI: http://dx.doi.org/10.2971/jeos.2016.16004]

Keywords: Thermal lens spectroscopy, heat equation, top-hat profile, thermal lensing

1 INTRODUCTION

Lasers are powerful tools for spectroscopic studies due to their specific properties such as narrow beam divergence, high degree of spatial and temporal coherence, well-defined polarization, and high intensity. One of the most sensitive spectroscopic techniques which is based on the laser induced heat is thermal lens spectroscopy (TLS) [1]. From superior applications of TLS, one can name the capability of detecting actinides at submicromolar concentrations in aqueous solution [2]. TLS is well-used to measure the optical absorption and thermal characteristics of materials [3]–[8].

Thermal lens (TL) effect was first discovered when Gordon et al. [9] observed a transient power and beam divergence change in the output of a helium-neon laser after placing transparent samples in the laser resonator. The thermal lens has been realized to be a photo-thermal effect arising from the fact that the refraction index is changed with temperature. A spatial distribution of temperature happens when a focused light beam passes through an absorbing medium. So, the change of refractive index with temperature, or dn/dT effect, turns the medium into a lens which is experienced by the probe beam [10]–[12]. The development of the thermal lens in the medium causes a spread in the beam and a drop in its intensity [13]. For a transparent sample, by measuring the beam divergence or intensity drop at the beam center with a small photo-detector placed at the other end of the sample, the thermal and optical properties of the sample can be measured [13, 14]. The so-called thermal lens spectroscopy is being used in many applications including material testing [15], combustion studies [16], plasma diagnostics [17], heat diffusion researches [18] and phase transitions studies [19, 20]. In some researches, such as Ref. [21], applications of TLS in food and environmental analysis have been reported.

Whinnery and Hu [22, 23] were pioneering authors who proposed a model to calculate the thermal lens. They treated the thermal lens as a perfect thin lens, that is, the thermal lens was approximated by a parabolic distribution. Sheldon et al. [11] presented a more completed model including the thermal lens aberrations. Their model has covered the single-beam as well as the mode-matched dual-beam TLS. Power [24] developed a mode-mismatched dual-beam TLS model for a short pulse excitation laser beam. Further study and development of models led to a more precise model in 1992 by Shen et al. [14]. They generalized the work of Sheldon et al. [11] for continuous wave (CW) mode-mismatched dual-beam TLS. It should be noted that the dual-beam TLS is more sensitive than single-beam method [3, 15]. This is because, in the dual-beam technique, one beam acts as the pump beam (absorbed by the sample) while the other beam acts as the probe (without significant absorption in the sample). Unlike the dual-beam TLS, the single-beam TLS technique is difficult to estimate the TL signal [25]. Furthermore, dual-beam mode-mismatched TLS is more sensitive than other methods, i.e. single-beam and dual-beam mode-matched TLS [26].

Bialkowski and Chartier [27] by developing the work of Shen et al. and considering the effects of optical geometry on the photo-thermal lens signal, presented a model in which, unlike to work of Shen et al., did not use the Fresnel diffraction integral [11, 28]. Their model was based on the assumption of cumulative electric-field phase shifts of a series of Gaussian refractive index perturbations caused by the photo-

Received October 01, 2015; revised ms. received December 13, 2015; published February 06, 2016

ISSN 1990-2573

thermal effect [27]. Nevertheless, this model did not possess the capability of application in dual-beam mode-mismatched TLS.

Further progress on TLS has led to introduce a top-hat beam excitation with pulsed beams as reported by Li et al. [29, 30]. They theoretically showed that with a top-hat excitation beam, the TL instrument is more sensitive than the Gaussian beam TL instrument, with a potential doubling of the sensitivity. Astrath et al. [15], in addition to present a numerical model for mode-mismatched TLS with a top-hat profile, showed that the experimental data are consistent very well with theoretical model and literature values of thermo-optical properties of LSCAS-2, ZBLAN and Soda-lime.

In all mentioned works, in particular those that are mostly related to this work, such as Refs. [9, 14, 15, 31], the sample was treated as an infinite medium in radial direction. This is a weakness for thermal model, because in factual situations, the samples are finite in radial direction, so that the heat energy flows into the ambience. From the theoretical point of view, if a sample is considered to be infinite while the heat source is in operation, at very large time, the temperature goes to infinity, i.e. the temperature is diverged. As stated by Gordon [9], the weakness of considering the sample as an infinite medium is that the temperature diverges at long enough times instead of converging to a steady-state value. Furthermore, a "Ln" term is appeared in basic model of TL signal which have to be ignored when fitting the TLS model on the experimental data [14]. To solve this problem, Shen et al. [32] derived a finite radius thermal model by using the finite radius Green's function presented by Carslaw and Jaeger [33]. However, this model led to a numerical model. Sabaeian and Nadgaran [34] more recently have presented a full analytical TLS model based on a thermal model for finite radius cylindrical samples exposed to a Gaussian excitation beam. They showed that at large enough time, the thermal model gets close to steady-state model, and therefore they concluded that this discrepancy on time has been removed. Their model could very well yield unknown thermo-optical data mostly closed to expected data of pure water and methylene blue.

As mentioned earlier, Astrath et al. [15] presented a TLS model with a top-hat excitation beam. Nevertheless, they used a numerical approach to reach a TLS signal. Due to the importance of top-hat TLS configuration which has been shown to be more sensitive than Gaussian one [3, 15], and since so far no analytical solution has been reported, therefore, we, in this work, present an analytical version for top-hat long transient dual-beam mode-mismatched TLS. The TLS model is well-known that contains two unknown parameters, namely θ and D, which with a good fit on experimental data, yields these unknown parameters. In order to confirm our model, we will use the expected data of LSCAS-2 reported in Ref. [15] to fit our model on experimental data of Astrath et al. The results show an excellent fit of our model with expected data on experimental data.

2 THEORY

2.1 Thermal model

The time-dependent heat equation governing the heat transfer in an isotropic medium is given by [32]:

$$c\rho\frac{\partial\left[\Delta T(r,t)\right]}{\partial t}-K\nabla^2\left[\Delta T(r,t)\right]=Q(r) \tag{1}$$

where $\Delta T(r,t)$ is the temperature change relative to ambience, and c,ρ and K are the specific heat, mass density, and thermal conductivity of the sample, respectively. For a continuous-wave excitation beam which is switched on at $t=0$, the initial condition of $\Delta T(r,t)=0$ is appropriated. Also, for a cylindrical finite radius sample, which is large enough compared to the excitation beam spot size, the boundary conditions of $\Delta T(r=a,t)=0$ is used. $Q(r)$ is the heat source and since in this work we are going to consider a top-hat excitation beam for a low absorbent media, it is assumed to be [15]:

$$Q(r)=\frac{P_eA_e\phi}{\rho c\pi\omega_e^2}U(\omega_e-r) \tag{2}$$

where $U(\omega_e-r)$ is a unit-step function, P_e is the excitation beam power, A_e is the optical absorption coefficient of the sample at the excitation beam wavelength, ω_e is the excitation beam radius at the sample, $\phi=1-\eta\lambda_e/\langle\lambda_{em}\rangle$ is the fraction of absorbed pump which is converted to the heat with λ_e as the excitation beam wavelength, $\langle\lambda_{em}\rangle$ the average wavelength of the fluorescence emission, and η as the fluorescence quantum efficiency [15].

In order to solve Eq. (1) for a cylindrically-shaped sample with a radius of a and a length of l, we start by rewriting Eq. (1) in the circular cylindrical coordinates as

$$\begin{aligned}&c\rho\frac{\partial\left[\Delta T(r,t)\right]}{\partial t}-K\left(\frac{\partial^2}{\partial r^2}+\frac{1}{r}\frac{\partial}{\partial r}\right)\left[\Delta T(r,t)\right]\\&=Q_0U(\omega_{0e}-r)\end{aligned} \tag{3}$$

where $Q_0=P_eA_e\phi/(\rho c\pi\omega_e^2)$.

In the next two subsections, we will consider two cases of infinite radius sample and finite radius sample and find solutions for temperature distribution. We will show although our approach towards finding a solution for temperature distribution for infinite radius sample is quite difference with the previous works done, however, it eventually coincides exactly on Gordon's method (for top-hat heat source), having the weakness of divergence at long enough time. Therefore, the model of finite radius sample which is shown to not diverge and coincides on the steady-state solution at long elapse time is chosen and the TLS model is based on it.

2.1.1 Infinite radius approach

In order to solve Eq. (3) by assumption of an infinite radius sample, the temperature difference, $\Delta T(r,t)$, in the cylindrical coordinates is expanded in terms of orthogonal Bessel functions as:

$$\Delta T(r,t)=\int_0^{+\infty}J_0(kr)\tau(k,t)dk \tag{4}$$

where $J_0(kr)$ is the zero-order Bessel function and $\tau(k,t)$ is an unknown function to be determined. Having regarded to the

above solution, the second term in Eq. (3) would be equal to $K\int_0^{+\infty}\tau(k,t)[-k^2J_0(kr)]dk$. This allows us to rewrite Eq. (3) as:

$$\int_0^{+\infty} J_0(kr)\left[\rho c\frac{d\tau(k,t)}{dt}+Kk^2\tau(k,t)\right]dk=Q_0U(\omega_{0e}-r) \quad (5)$$

Multiplying both sides of Eq. (5) by $rJ_0(k'r)$ and integrating over r from 0 to ∞, we end up with:

$$\frac{d\tau(k,t)}{dt}+Dk^2\tau(k,t)=\frac{Q_0\omega_eJ_1(k\omega_e)}{\rho c} \quad (6)$$

where $D = K/\rho c$ is the thermal diffusivity and $J_1(x)$ is the first order Bessel function. With initial condition of $\Delta T(r,t=0)=0$, the solution of Eq. (6) is as follows:

$$\tau(k,t)=\frac{Q_0\omega_eJ_1(k\omega_e)}{K}\left[1-\exp(-Dk^2t)\right] \quad (7)$$

So by substituting Eq. (7) in Eq. (4), the temperature difference, $\Delta T(r,t)$, is obtained as:

$$\Delta T(r,t) = \frac{1}{4}\frac{Q_0\omega_e^2}{K}\left[\int_0^{+\infty}J_0(kr)\frac{1}{k}e^{-\alpha k^2}dk-\int_0^{+\infty}J_0(kr)\frac{1}{k}e^{-\beta k^2}dk\right] \quad (8)$$

where $\alpha = \omega_e^2/8$ and $\beta = \omega_e^2/8 + Dt$. By solving the above integration with a laborious approach, finally we end up with the following solution:

$$\Delta T(r,t)=\frac{Q_0\omega_e^2}{8K}\left[Ei\left(1,\frac{2r^2}{\omega_e^2+8Dt}\right)-Ei\left(1,\frac{2r^2}{\omega_e^2}\right)\right] \quad (9)$$

where $Ei(a,z)$ is the exponential integral. Eq. (9) is exactly the equation that was obtained in the work of Gordon et al. [9]. A detailed discussion of above solution have been come in Ref. [34]. As Gordon et al. have reported, this solution has the weakness of divergence at large enough time instead of closing to steady-state solution. In the next subsection, we derive a solution for temperature distribution with a factual assumption of finite radius for sample. As we will see, this solution is free of that shortage seen in infinite solution.

2.1.2 Finite radius approach

In this subsection, similar to that done to solve Eq. (3), the temperature difference, $\Delta T(r,t)$, is expanded in terms of orthogonal Bessel functions in the cylindrical coordinates, but by using a summation instead of an integration, as:

$$\Delta T(r,t)=\sum_{n=1}^{\infty}J_0\left(r\alpha_n/a\right)\tau_n(t) \quad (10)$$

where $J_0\left(r\alpha_n/a\right)$ is the zero-order Bessel function and $\tau_n(t)$ is an unknown function to be determined. If $a >> \omega_e$ (e.g. $a/\omega_e \sim 10$), the assumption of constant temperature at the sample boundaries requires that α_n's being the roots of zero-order Bessel function. With above primary solution, the second term in Eq. (3) would be equal to $(\alpha_n/a)^2 J_0\left(r\alpha_n/a\right)$. This allows us to separate the variables r and t in Eq. (3) as is done as follows:

$$\sum_{n=1}^{\infty}J_0\left(r\alpha_n/a\right)\left[\rho c\frac{d\tau_n(t)}{dt}+\frac{K\alpha_n}{a^2}\tau_n(t)\right]=Q_0U(\omega_e-r) \quad (11)$$

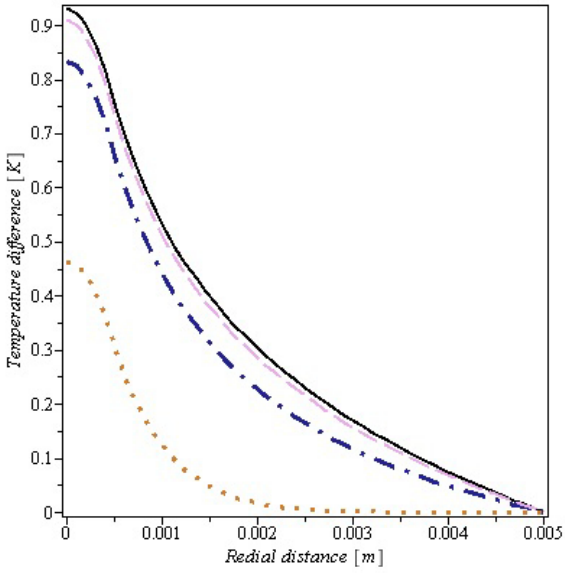

FIG. 1 Temperature distribution versus the radial distance. From bottom to top, the curves shows $\Delta T(r,t)$ for t = 1 s (dotted curve), t = 10 s (dashed-dot curve), t = 20 s (dashed curve), and t = 200 s (solid curve), respectively.

Multiplying both sides of Eq. (11) by $rJ_0\left(r\alpha_{n'}/a\right)$ and integrating over r from 0 to a, we end up with

$$\rho c\frac{d\tau_n(t)}{dt}+\frac{K\alpha_n}{a^2}\tau_n(t)=\frac{2Q_0}{a^2J_1^2(\alpha_n)}I_n \quad (12)$$

where I_n is defined as

$$I_n=\int_0^a U(\omega_e-r)J_0\left(r\alpha_n/a\right)rdr = \int_0^{\omega_e}J_0\left(r\alpha_n/a\right)rdr=\frac{a\omega_eJ_1\left(\omega_e\alpha_n/a\right)}{\alpha_n} \quad (13)$$

Eq. (12) is a linear first-order differential equation and has a straightforward solution of

$$\tau_n(t)=\frac{2Q_0I_n}{K\alpha_n^2J_1^2(\alpha_n)}[1-\exp(-\frac{D\alpha_n^2}{a^2}t)] \quad (14)$$

with initial condition of $\Delta T(r,t=0)=0$.

Figure 1 shows the temperature distribution, $\Delta T(r,t)$, obtained in this subsection at several times including long elapsed time and compares the result with its steady state regime. The steady-state solution can be found in Refs. [9, 34]. The parameters used for plotting the curves are as follow: $\omega_e = 275$ μm, $P_e = 66$ mW, $A_e = 1.70$ cm^{-1}, $\eta = 0.84$, $\lambda_e = 532$ nm, $<\lambda_{em}>= 1064$ nm, $D = K/\rho c = 5.7\times10^{-3}$ cm^{2}s^{-1},$a = 5$ mm, $l = 1.5$ mm which are taken from Refs. [3, 15]. The number of 50 terms has been retained in the summation of Eq. (10) to reach an accurate solution and to agree with numerical solution. Figure 1 reports a reasonable behavior for temperature at long elapsed time, that is, the temperature approaches its steady state.

2.2 Thermally induced phase shift

Unlike the liquids, in the solid samples, besides the dn/dT effect, the end effect and thermal stresses result from the local inhomogeneous temperature rise inside the sample. In the TL

experiments, the end effect causes a bulging of the end faces through axial expansion of the sample [35]. Also the cooler outer part of the sample prevents the expansion of its hotter central region generates the stresses [36]. These effects are discussed in detail in the literature [36]–[39]. In these studies, in order to account for these effects, dS/dT is used instead of dn/dT. These effects are accounted by the first, second and third term in Eq. (16). So, in solid samples, such as LSCAS-2, the temporal and radial distributions of the temperature rise inside the sample induces a refractive index gradient, acting as an optical element and causing a thermal induced phase shift to the probe beam that for thin-disk or long-rod geometry, can be written as follows [36, 39]:

$$\varphi(r,t) = k_p l \frac{\partial S}{\partial T} \times [\Delta T(r,t) - \Delta T(r=0,t)] \qquad (15)$$

where $\partial S/\partial T$ that depends on the geometry of the sample is the temperature coefficient of the optical path length at the probe beam wave number, k_p. For sample with thin-disk geometry, the plane-stress approximation can be used, and the thermal coefficient of optical path can be written as:

$$\frac{\partial S}{\partial T} = \frac{\partial n}{\partial T} + (n-1)(1+v)\alpha + \frac{n^3 E\alpha}{4}(q_{\parallel} + q_{\perp}) \qquad (16)$$

where α is the linear thermal-expansion coefficient, E is the Young's modulus, v is the Poisson's ratio, $q_{\parallel}$ and $q_{\perp}$ are, respectively, the stress-optical coefficients for the parallel and perpendicular orientation relative to excitation beam polarization [36]. Using temperature distribution calculated in Eqs. (10) and (14), the phase difference is obtained as

$$\varphi(r,t) = k_p l \frac{\partial S}{\partial T} \sum_{n-1}^{\infty} \tau_n(t) \left[J_0\left(r\alpha_n/a\right) - 1\right] \qquad (17)$$

The variations of thermally induced phase shift versus r are plotted in Figure 2 for three different times which shows the typically small value for the thermally induced phase shifts. This is the case for low absorbent samples. Here, the parameters of Figure 1 are used.

One of the outstanding points of the present work is inclusion of all aberrations term in the thermal phase shift which is brough in thermal lens signal calculated in the next section.

3 Thermal lens signal

Figure 3 illustrates a schematic diagram of dual-beam mode-mismatched TLS setup. In this setup, a sample is exposed to two laser beams having beam waists of ω_{1p}(for probe beam) and ω_e (for excitation beam).The details of this setup has been explained in Ref. [34]. If the sample is located at z, using the Fresnel diffraction theory, the propagation of a TEM_{00} Gaussian probe beam through the sample to the detector plane can be obtained as [14]:

$$U_2(z+z_2,t) = C\int_0^{\infty} \exp[-(1+iV)g] \times \exp(-i\varphi)dg \qquad (18)$$

where $C = B[ik_p\omega_{1p}^2/(2z_2)]\exp(-ik_p z_2)$, z_2 is the distance from the sample to the detector and can be written as

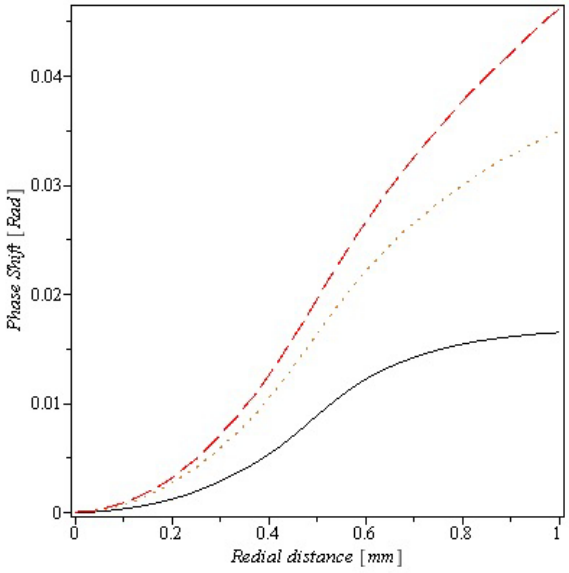

FIG. 2 Thermal phase shift versus the radial distance for t =0.1 s (solid curve), t = 0.5 s (dotted curve), and t = 10 s (dashed curve). The parameters used are the same as in Figure 1.

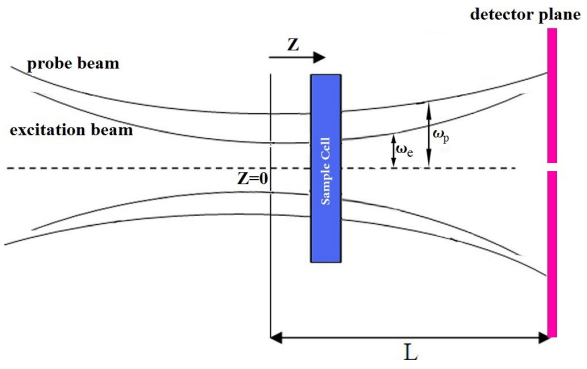

FIG. 3 A schematic diagram of the probe and excitation beams in a dual-beam mode-mismatched TLS setup. The sample cell is exposed to a laser beam with a spot size of ω_e. The beam spot size of probe beam over the sample is ω_{1p}. The detector plane is located at the distance L from the origin (z = 0) [34].

$z_2 = L - z$, where L is the detector position shown in the Figure 3,

$$B = \sqrt{2P_p/\pi\omega_{1p}^2}\exp(-ik_p z)\ ,$$
$$V = z/z_p + z_p[1+(z/z_p)^2]/(L-z)\ ,$$
$$z_p = \pi\omega_{0p}^2/\lambda_p\ ,\quad g = (r/\omega_{1p})^2$$

and ω_{0p} is the probe beam waist.

To the best of our knowledge, the analytical solution of Eq. (18), does not exist [34]. However, for a low absorbent case, which is the case in our work, we can used the approximation of $\exp(-i\varphi) \approx 1 - i\varphi$ [11, 14] where φ contains aberration terms. The higher-order expansion terms are necessary for accurate signal prediction only in highly absorbing samples or when high-power excitation source are used [27]. Furthermore, Sheldon et al. [11] argued that because the induced phase shift in the most photo-thermal lens experiments is much less than unit, higher-order series approximations are not necessary. We have shown earlier that this phase shift is small enough (see Figure 2) for safe use of this approximation.

After calculating $U_2(z+z_2,t)$ via Eq. (18), then multiplying by $U_2(z+z_2,t)*$, we get the on-axis normalized beam intensity at the location of the detector as:

$$\frac{I(t)}{I(0)} = \left(1-\theta\sum_{n=1}^{\infty}\frac{J_1(\frac{\alpha_n}{m'})\left(1-e^{(-\beta_n^2 t/t_c)}\right)}{\alpha_n^2 J_1^2(\alpha_n)} \cdot e^{(-\delta\alpha_n^2)}\sin(\alpha_n^2\delta V)\right)^2 + \left(\theta\sum_{n=1}^{\infty}\frac{J_1(\frac{\alpha_n}{m'})\left(1-e^{(-\beta_n^2 t/t_c)}\right)}{\alpha_n^2 J_1^2(\alpha_n)} \cdot \left(1-e^{(-\delta\alpha_n^2)}\cos(\alpha_n^2\delta V)\right)\right)^2 \quad (19)$$

where $\theta \equiv P_e A_e l\,\phi\,(\partial S/\partial T)\,(4m'/\rho c K\lambda_p)$, $m' = a/\omega_e$, $\delta = \omega_{1p}^2/[4a^2(1+V^2)]$, $\beta_n = \alpha_n\omega_e/2a$ and $t_c = \omega_e^2/4D$. In the case where the absorption is very low, i.e. when $\theta \ll 1$, we can ignore the terms including θ^2 in Eq. (19) safely. So by expanding Eq. (19) and ignoring θ^2 term, we have

$$\frac{I(t)}{I(0)} = 1-2\theta\sum_{n=1}^{\infty}\frac{J_1(\alpha_n/m')[1-e^{(-\beta_n^2 t/t_c)}]}{\alpha_n^2 J_1^2(\alpha_n)} \cdot e^{-\delta\alpha_n^2}\sin(\alpha_n^2\delta V) \quad (20)$$

3.1 Confirmation of model with experimental data

In order to validate our analytical model, we used the expected dada for θ and D reported in the literature [40] to fit our model on experimental data of Astrath et al. [15] obtained from LSCAS-2. As mentioned, Astrath et al. [15] in their work developed a numerical method to extract physical properties of the sample.

The parameters used in the work of Astrath et al. [15] are as follows: excitation laser spot size at cell $\omega_e = 275$ μm, container length $l = 1.5$ mm, probe laser spot size at cell $\omega_{1p} = 920$ μm, excitation laser power $P_e = 66$ mW, absorption coefficient $A_e = 1.70$ cm^{-1}, $V = 15.2$, and $Z_2 = 5$ m. Figure 4 shows the experimental data of Astrath et al. (circles) which are $I(t)/I_0$ at various times. The data of Astrath et al. are 155 points which were extracted point-by-point from their original paper [15]. In Figure 4, solid line shows our model (Eq. (20)) with $\Theta = -7.0$ [W^{-1}] ($\Theta = \theta\rho c/(P_e l A_e 4m')$) and $D = 5.8\times10^{-3}$[cm^2 / s] which are given in Ref. [40]. The fitting of our model (with expected Θ and D) on experimental data of Astrath et al. reveals an excellent agreement. The expected data and those extracted through numerical model of Astrath et al. are listed in Table 1. Apart from reporting an analytical model, our model shows a better fitting on experimental data.

4 CONCLUSION

In conclusion, in this work, we have presented a full analytical model for top-hat CW excitation beam for dual-beam mode-mismatched thermal lens spectroscopy (TLS). The model was based on an analytical thermal model for finite radius sample without divergence at long elapsed times which is reported in the previous model. Furthermore, for low absorbent samples, all aberration terms associated in thermal lens were taken into account in Fresnel integration. Our full analytical model has been fitted very well, with expected date for two unknown parameters in the model, on the experimental data for LSCAS-2 sample. In this regard, this analytical model can be very well suited for low absorption materials when more sensitive TLS with top-hat excitation beams is needed for calculation of thermo-optical parameters.

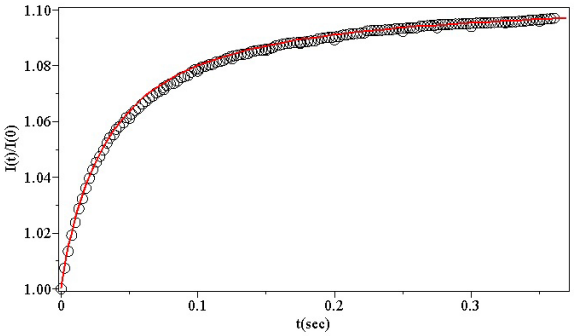

FIG. 4 Experimental data [15] (circles) along with fitting results of our model (solid curve) for the LSCAS-2.

5 ACKNOWLEDGMENTS

The authors would like to extend their special thanks and appreciations to the Shahid Chamran University of Ahvaz, Iran for supporting this work.

Samples	D [10^{-3}cm^2/s]	Θ [W^{-1}]*
The work of Astrath et al.	5.7	-7.1
Expected data [40]	5.8	-7.0

*$\Theta = (\delta S/\delta T)\phi/K\lambda_P$

TABLE 1 Experimental data from Astrath et al.'s numerical work [15] and expected data [40] for LSCAS-2.

References

[1] M. L. Baesso, J. R. D. Pereira, A. C. Bento, and A. J. Palangana, "Thermal lens spectrometry to study complex fluids," Braz. J. Phys. **28**, (1998).

[2] D. A. Wruck, R. E. Russo, and R. J. Silva, "Thermal lens spectroscopy of plutonium using a laser diode and fiber optics," J. Alloy. Compd. **213–214**, 481–483 (1994).

[3] N. G. C. Astrath, J. Shen, M. L. Baesso, F. B. G. Astrath, L. C. Malacarne, P. R. B. Pedreira, A. C. Bento, et al., "Material characterization with top-hat cw laser induced photothermal techniques: A short review," J. Phys. Conf. Ser. **214**, 012014 (2010).

[4] N. Astrath, F. Astrath, J. Shen, J. Zhou, K. Michaelian, C. Fairbridge, L. Malacarne, et al., "Arrhenius behavior of hydrocarbon fuel photochemical reaction rates by thermal lens spectroscopy," Appl. Phys. Lett. **95**, 191902 (2009).

[5] A. Marcano, H. Cabrera, M. Guerra, R. A. Cruz, C. Jacinto, and T. Catunda, "Optimizing and calibrating a mode-mismatched thermal lens experiment for low absorption measurement," JOSA B **23**, 1408–1413 (2006).

[6] C. Jacinto, A. Andrade, T. Catunda, S. Lima, and M. Baesso, "Thermal lens spectroscopy of Nd: YAG," Appl. Phys. Lett. **86**, 34104–34104 (2005).

[7] C. Jacinto, T. Catunda, D. Jaque, L. Bausa, and J. García-Solé, "Thermal lens and heat generation of Nd: YAG lasers operating at 1.064 and 1.34 μm," Opt. Express **16**, 6317–6323 (2008).

[8] C. Jacinto, D. N. Messias, A. A. Andrade, S. Lima, M. L. Baesso, and T. Catunda, "Thermal lens and Z-scan measurements: Thermal and optical properties of laser glasses–A review," J. Non-Cryst. Solids **352**, 3582–3597 (2006).

[9] J. P. Gordon, R. C. C. Leite, R. S. Moore, S. P. S. Porto, and J. R. Whinnery, "Long-Transient Effects in Lasers with Inserted Liquid Samples " J. Appl. Phys. **36**, 3–8 (1965).

[10] R. Escalona, "Study of a convective field induced by thermal lensing using interferometry," Opt. Commun. **281**, 388–394 (2008).

[11] S. J. Sheldon, L. V. Knight, and J. M. Thorne, "Laser-induced thermal lens effect: a new theoretical model," Appl. Optics **21**, 1663–1669 (1982).

[12] J. Hung, A. Marcano O, J. Castillo, J. González, V. Piscitelli, A. Reyes, and A. Fernández, "Thermal lensing and absorbance spectra of a fluorescent dye solution," Chem. Phys. Lett. **386**, 206–210 (2004).

[13] L. C. M. Miranda, "On the use of the thermal lens effect as a thermo-optical spectroscopy of solids," Appl. Phys. A **32**, 87–93 (1983).

[14] J. Shen, R. D. Lowe, and R. D. Snook, "A model for cw laser induced mode-mismatched dual-beam thermal lens spectrometry," Chem. Phys. **165**, 385–396 (1992).

[15] N. G. Astrath, F. B. Astrath, J. Shen, J. Zhou, P. R. Pedreira, L. C. Malacarne, A. C. Bento, et al., "Top-hat cw-laser-induced time-resolved mode-mismatched thermal lens spectroscopy for quantitative analysis of low-absorption materials," Opt. Lett. **33**, 1464–1466 (2008).

[16] N. G. C. Astrath, F. B. G. Astrath, J. Shen, J. Zhou, K. H. Michaelian, C. Fairbridge, L. C. Malacarne, et al., "Arrhenius behavior of hydrocarbon fuel photochemical reaction rates by thermal lens spectroscopy," Appl. Phys. Lett. **95**, 191902 (2009).

[17] J. Bernal-Alvarado, M. Sosa, R. Mayén-Mondragón, J. M. Yánez-Limón, R. Flores-Farías, F. Hernández-Cabrera, and P. Palomares, "Mismatched Mode Thermal Lens for Assessing Thermal Diffusivity of Serum and Plasma from Human Blood," Instrum. Sci. Technol. **34**, 99–105 (2006).

[18] R. Gutiérrez Fuentes, J. F. Sánchez Ramírez, J. L. Jiménez Pérez, J. A. Pescador Rojas, E. Ramón-Gallegos, and A. Cruz-Orea, "Thermal Diffusivity Determination of Protoporphyrin IX Solution Mixed with Gold Metallic Nanoparticles," Int. J. Thermophys. **28**, 1048–1055 (2007).

[19] C. Jacinto, T. Catunda, D. Jaque, J. Garcia Sole, and A. A. Kaminskii, "Thermal lens spectroscopy through phase transition in neodymium doped strontium barium niobate laser crystals," J. Appl. Phys. **101**, 023113–023116 (2007).

[20] R. Mayén-Mondragón and J. M. Yáñez-Limón, "Study of blue phases transition kinetics by thermal lens spectroscopy in cholesteryl nonanoate," Rev. Sci. Instrum. **77**, 044903 (2006).

[21] M. Franko, "Recent applications of thermal lens spectrometry in food analysis and environmental research," Talanta **54**, 1–13 (2001).

[22] C. Hu, and J. R. Whinnery, "New Thermooptical Measurement Method and a Comparison with Other Methods," Appl. Optics **12**, 72–79 (1973).

[23] J. R. Whinnery, "Laser measurement of optical absorption in liquids," Accounts Chem. Res. **7**, 225–231 (1974).

[24] J. F. Power, "Pulsed mode thermal lens effect detection in the near field via thermally induced probe beam spatial phase modulation: a theory," Appl. Optics **29**, 52–63 (1990).

[25] P. Kumar, S. Dinda, and D. Goswami, "Effect of molecular structural isomers in thermal lens spectroscopy," Chem. Phys. Lett. **601**, 163–167 (2014).

[26] R. D. Snook, and R. D. Lowe, "Thermal lens spectrometry. A review," Analyst **120**, 2051–2068 (1995).

[27] S. E. Bialkowski, and A. Chartier, "Diffraction effects in single- and two-laser photothermal lens spectroscopy," Appl. Optics **36**, 6711–6721 (1997).

[28] S. E. Bialkowski, *Photothermal Spectroscopy Methods for Chemical Analysis* (Wiley-Blackwell, Haboken, 1996).

[29] B. Li, and E. Welsch, "Probe-beam diffraction in a pulsed top-hat beam thermal lens with a mode-mismatched configuration," Appl. Optics **38**, 5241–5249 (1999).

[30] B. Li, S. Xiong, and Y. Zhang, "Fresnel diffraction model for mode-mismatched thermal lens with top-hat beam excitation," Appl. Phys. B **80**, 527–534 (2005).

[31] S. Wu and N. J. Dovichi, "Fresnel diffraction theory for steady-state thermal lens measurements in thin films," J. Appl. Phys. **67**, 1170–1182 (1990).

[32] J. Shen and R. D. Snook, "A radial finite model of thermal lens spectrometry and the influence of sample radius upon the validity of the radial infinite model," J. Appl. Phys. **73**, 5286–5288 (1993).

[33] H. S. J. J. C. Carslaw, *Conduction of heat in solids* (Clarendon Press, Oxford, 1959).

[34] M. Sabaeian and H. Nadgaran, "An analytical model for finite radius dual-beam mode-mismatched thermal lens spectroscopy," J. Appl. Phys. **114**, 133102–133107 (2013).

[35] H. Nadgaran and M. Sabaian, "Pulsed pump: Thermal effects in solid state lasers under super-Gaussian pulses," Pramana - J. Phys. **67**, 1119–1128 (2006).

[36] A. A. Andrade, T. Catunda, I. Bodnar, J. Mura, and M. L. Baesso, "Thermal lens determination of the temperature coefficient of optical path length in optical materials," Rev. Sci. Instrum. **74**, 877–880 (2003).

[37] S. M. Lima, J. A. Sampaio, T. Catunda, A. C. Bento, L. C. M. Miranda, and M. L. Baesso, "Mode-mismatched thermal lens spectrometry for thermo-optical properties measurement in optical glasses: a review," J. Non-Cryst. Solids **273**, 215–227 (2000).

[38] M. L. Baesso, J. Shen, and R. D. Snook, "Mode-mismatched thermal lens determination of temperature coefficient of optical path length in soda lime glass at different wavelengths," J. Appl. Phys. **75**, 3732–3737 (1994).

[39] L. C. Malacarne, N. G. C. Astrath, and M. L. Baesso, "Unified theoretical model for calculating laser-induced wavefront distortion in optical materials," JOSA B **29**, 1772–1777 (2012).

[40] E. Peliçon, J. H. Rohling, A. N. Medina, A. C. Bento, M. L. Baesso, D. F. de Souza, S. L. Oliveira, et al., "Temperature dependence of fluorescence quantum efficiency of optical glasses determined by thermal lens spectrometry," J. Non-Cryst. Solids **304**, 244–250 (2002).